Simple tools for complex phenomena: Viscoelastic phase separation captured by disconnectable springs

Takeaki Araki and Hajime Tanaka
Institute of Industrial Science, University of Tokyo, Tokyo 153-8505, Japan
(Received 2 February 2005; revised manuscript received 25 July 2005; published 21 October 2005)

Viscoelastic phase separation is characterized by the formation of a transient gel upon phase separation. A transient gel state is widely observed in complex fluids including polymer solutions, colloidal suspensions, and protein solutions, but its physical description is quite difficult due to its intrinsically nonequilibrium nature. We have modeled this transient gel state using a type of Brownian dynamics simulation in which coarse-grained particles interacting with a Lennard-Jones potential are connected by elastic springs, which can be disconnected with the probability controlled by the ratio of the stored elastic energy to the thermal energy. The simulations well reproduce pattern evolution in a transient gel of a polymer solution. Our simulations indicate that domain morphology is controlled by two key physical factors: (i) the ratio between the nucleation and growth rates of domains of the less viscoelastic phase and (ii) the fragility of the transient gel.

DOI: 10.1103/PhysRevE.72.041509 PACS number(s): 64.75.+g, 05.70.Fh, 61.25.Hq, 61.41.+e

I. INTRODUCTION

Viscoelastic phase separation (VPS) is a type of phase separation observed in a mixture of slow and fast components [1–7]. One of the most remarkable features of VPS is networklike pattern formation of the more viscoelastic phase even if it is a minority phase. VPS proceeds as follows: (i) transient gel formation just after the temperature quench, (ii) selective nucleation of the solvent-rich phase in the transient gel after some incubation period, even though this phase is a majority phase, (iii) gel-like volume shrinking of the polymer-rich phase, (iv) transient formation of a networklike structure, and (v) phase inversion and pattern relaxation to a droplet morphology in the late stage. We proposed that VPS may be universally observed for "dynamically asymmetric mixtures," such as polymer solutions [1–3], mixtures of components having different T_g [8], colloidal dispersions [7], microemulsions [9], and protein solutions [10].

For VPS, many concepts, such as self-similarity and the resulting dynamical scaling law, which are useful for predicting the domain morphology of normal phase separation, cannot be applied. Since the late-stage phase-separation process of VPS is a result of complex nonlinear couplings among concentration, stress, and velocity fields, it is quite difficult to predict the pattern evolution of VPS analytically. Thus, numerical simulations have played a crucial role in the understanding of the physical mechanisms behind the phenomena. So far numerical simulations based on a two-fluid model [11–17], a concentration-dependent mobility [18,19], and molecular dynamics [20,21] have been performed. However, the most difficult theoretical problem arises from the fact that the transient gel formed just after the temperature quench is intrinsically in a nonequilibrium state. We need a constitutive equation describing the transient gel state, but there are no theories for the rheological behavior of a system in an unstable state of a mixture. We recently proposed a specific form of the constitutive equation for the transient gel state, focusing on the role of the bulk stress stemming from the connectivity of the network [4,5]. We introduced a step function into the bulk modulus to express the fact that the connectivity suppresses the diffusion, but if the connectivity is lost by the breakup of bonds the bulk modulus disappears. Numerical simulations based on this model [12,13] capture some essential features of the pattern evolution and demonstrate the importance of the role of the bulk stress, i.e., the connectivity of the transient gel. However, the highly coarse-grained description does not tell us about the elementary process of the coarsening of the transient gel. Here we propose another type of coarse-grained simulation, namely, we express the transient gel state by coarse-grained Brownian particles connected by disconnectable springs. In this paper we will seek physical factors controlling the network morphology of VPS on the basis of a disconnectable spring model.

II. COARSE-GRAINING DESCRIPTION OF A TRANSIENT GEL

We have recently reported that aggregating colloidal particles form a chainlike structure with the help of interparticle hydrodynamic interaction, and further form a network structure [5,22]. This network structure can be regarded as a transient gel, which plays a key role in VPS [4,5]. Here, we consider the elementary process of spontaneous destruction of a transient gel state under self-generated mechanical stress. In the following, we coarse-grain a chainlike aggregate of colloidal particles and express it as a disconnectable spring.

Let us consider a one-dimensional chain consisting of N_p particles, which are under tension [see Fig. 1(a)]. We assume that particles are interacting with each other via a harmonic potential $U_p(r)=[-\epsilon_p+\kappa_p(r-b)^2/2]\Theta(r_c-r)$, where ϵ_p, b, and κ_p are the strength of the potential, the natural length of the harmonic interaction, and the spring constant, respectively. This potential is set to be zero for $r>r_c$, where $r_c=\sqrt{2\epsilon_p/\kappa_p}+b$. Here, the suffix p indicates a physical value related to the particle forming the chain [see the small particle in Fig. 1(a)]. Figure 1(b) shows the breakup process of

 ©2005 The American Physical Society

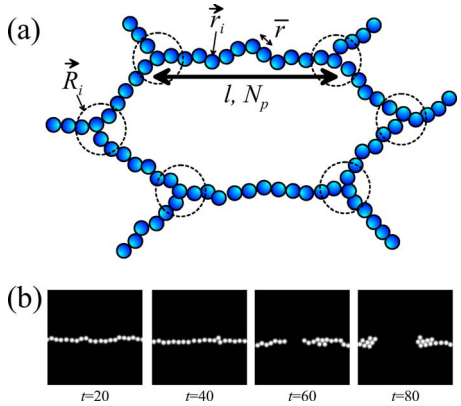

FIG. 1. (Color online) (a) Schematic figure of a network structure composed of colloidal particles. In our simulation method, this network consisting of small particles is approximated by pseudoparticles (dashed circles) connected by disconnectable springs. (b) An elementary process of disconnection of a particle chain simulated by Brownian dynamics simulation of Lennard-Jones particles. Initially particles are connected to form a chain. The disconnection process of this chain is simulated by solving the equation of motion $\zeta_p d\vec{r}_i/\mathrm{dt}=-(\partial/\partial\vec{r}_i)\Sigma_j U_p(|\vec{r}_i-\vec{r}_i|)+\vec{\xi}_i^p(t)$, with $\langle\vec{\xi}_i^p(t):\vec{\xi}_j^p(t')\rangle=2T\zeta_p\delta_{ij}\delta(t-t')\boldsymbol{I}$, where ζ_p is the friction constant. As shown above, the particle chain is eventually disconnected by thermal fluctuations.

a thermally fluctuating chain composed of particles, which is simulated by Brownian dynamics simulation. The chain is fluctuating due to thermal noise; thus, it is similar to a thermally fluctuating polymer chain whose ends are stretched. Unlike a polymer where monomers are permanently connected by covalent bonds, however, our chain has a finite disconnection probability and thus is eventually disconnected under the action of stress. The disconnection is irreversible and thus disconnected chains never reconnect again. The breakup process is probabilistic and can be regarded as a thermally activated process.

Next we estimate the disconnection rate of the above chain. If we consider only the interaction between nearest-neighbor particles, the chain can be described by a bead-spring model of a flexible polymer. Its free energy is given by [23]

$$\frac{\mathcal{F}}{N_p}=\frac{\kappa_p}{2}\int d\vec{u}(|\vec{u}|-b)^2 f(\vec{u})+T\int d\vec{u} f(\vec{u})\ln f(\vec{u}) - T\vec{\lambda}\cdot\left(\int d\vec{u}\vec{u}f(\vec{u})-\frac{\vec{l}}{N_p b}\right)-T\mu\left(\int d\vec{u}f(\vec{u})-1\right). \tag{1}$$

Here $f(\vec{u})$ is the distribution function of the relative vector between neighboring particles, $\vec{u}(=\vec{r}_{i+1}-\vec{r}_i)$, and $\vec{l}$ is the end-to-end vector of the chain, which is expressed as $\vec{l}=\vec{r}_{N_p}-\vec{r}_0$. T is the temperature and the Boltzmann constant k_B is set to unity. The first and second terms of Eq. (1) represent the elastic energy of springs and the entropy of chain conformation, respectively. μ and $\vec{\lambda}$ are the Lagrange multipliers, which are introduced to impose the following normalization conditions: $\int d\vec{u} f(\vec{u})=1$ and $\int d\vec{u}\,\vec{u}f(\vec{u})=\vec{l}/(N_p b)$, respectively. Minimization of Eq. (1) in terms of $f(\vec{u})$ (i.e., $\delta\mathcal{F}/\delta f=0$) leads to $f(\vec{u},\vec{\lambda},\kappa_p)=\exp[\vec{\lambda}\cdot\vec{u}-(\kappa_p/2T)(|\vec{u}|-b)^2]/Z(\vec{\lambda},\kappa_p)$. $Z(\vec{\lambda},\kappa_p)$ is a normalization factor given by

$$Z(\vec{\lambda},\kappa_p)=\int d\vec{u}\exp\left(\vec{\lambda}\cdot\vec{u}-\frac{\kappa_p}{2T}(|\vec{u}|-b)^2\right) \approx 4\pi\sqrt{\frac{2\pi T}{\kappa_p}}e^{T\lambda^2/2\kappa_p}\left(\frac{b}{\lambda}\sinh(\lambda b)+\frac{T}{\kappa_p}\cosh(\lambda b)\right). \tag{2}$$

From the relation $(\partial/\partial\vec{\lambda})\ln Z=\vec{l}/(N_p b)$, we obtain

$$l=N_p b\frac{(2T\lambda/\kappa_p b-1/\lambda b)\sinh(\lambda b)+(1+T^2\lambda^2/\kappa_p^2 b^2)\cosh(\lambda b)}{\sinh(\lambda b)+(T\lambda/\kappa_p b)\cosh(\lambda b)}. \tag{3}$$

The averaged elastic energy of a spring is obtained as

$$E=-T\kappa_p\frac{\partial}{\partial\kappa_p}\ln Z =\frac{T}{2}\frac{(1+T\lambda^2/\kappa_p)\sinh(\lambda b)+(3T\lambda/\kappa_p b+T^2\lambda^3/\kappa_p^2 b)\cosh(\lambda b)}{\sinh(\lambda b)+(T\lambda/\kappa_p b)\cosh(\lambda b)}. \tag{4}$$

Since the extensional stress acts on each particle due to the chain entropy and the spring elasticity, the average interparticle distance $\bar{r}$ becomes larger than the most probable separation $r=b$. Note that $N_p\bar{r}$ gives the contour length of the chain; thus, $l<N_p\bar{r}$. We assume that the excess energy of the interparticle interaction is almost equal to the elastic energy stored by each spring [see Eq. (5)]. When the average interparticle separation $\bar{r}$ is larger than r_c, the chainlike configuration becomes unstable and the chain is eventually disconnected by thermal fluctuations. Since, on the other hand, such a configuration is metastable for $r<r_c$, a certain energy barrier has to be overcome when the chain is disconnected. Assuming that all springs are equally stretched, this energy barrier height is estimated as $\Delta E=[U_p(r_c)-U_p(b)]-E(l)-T\ln N_p$. Using this, the disconnection rate can be approximated as $p(l)=t_0^{-1}\exp[-\Delta E(l)/T]$, where t_0 is the characteristic time scale of the chain fluctuations and $t_0=\zeta_p/\pi^2\kappa_p$. t_0^{-1} corresponds to the attempt frequency for disconnection. Here the last term of ΔE occurs because the attempt frequency should be multiplied N_p times for a chain composed of N_p springs.

$T\vec{\lambda}$ gives the force acting on both chain ends. Since l and E are monotonic odd and even functions of λ, respectively, E should be an even function of l. This means the leading order term of l upon expansion is l^2. Thus, $\Delta E(l)$ can be approximated as

$$\Delta E(l) \approx E_0 - \frac{1}{2}\kappa l^2, \tag{5}$$

where $E_0=\epsilon_p-(T/2)(\kappa_p b^2+3T)/(\kappa_p b^2+T)-T\ln N_p$ and $\kappa=(6\kappa_p/N_p^2)T^2(5/3\kappa_p^2 b^4+T\kappa_p b^2+T^2)/(\kappa_p^2 b^4/3+2T\kappa_p b^2+T^2)^2$. The contribution of higher-order terms becomes significant for larger $\kappa_p b^2/T$, while the above derivation of Eq. (2) is not valid for smaller $\kappa_p b^2/T$. Thus, this description is valid for the intermediate range of $\kappa_p b^2/T$. We confirm numerically that for $2\lesssim\kappa_p b^2/T\lesssim 10$ the numerical accuracy of Eq. (2) is within 10% even for strongly stretched springs ($l\approx N_p b$).

Next we describe the coarse-grained model of a transient gel based on the above-described disconnectable springs. In the above, we consider the disconnection process of a chain of particles. Here we coarse-grain a network by replacing chains of small particles by disconnectable springs. We treat the cross-linking points $\{\vec{R}_i\}$ [large dashed circles in Fig. 1(b)] as particles. We assume for simplicity that the physical parameters such as ϵ and ζ, which will be defined below, are independent of those of the small particles. This coarse-graining model, which has no microscopic information on colloidal particles, can now be applied to transient gel states of various types of dynamically asymmetric mixtures including not only colloidal suspensions but also polymer solutions and protein solutions.

III. NUMERICAL SIMULATION METHOD

The time evolution of this network composed of particles connected by disconnectable springs is simulated by a Brownian dynamics simulation method. We treat motion of coarse-grained particles immersed in a solvent in the overdamped limit. Thus, effects of the solvent are incorporated by a hydrodynamic drag force and a random Brownian force acting on the particles. The equation of motion for particle i is then given by

$$\zeta\frac{d}{dt}\vec{R}_i = -\frac{\partial}{\partial\vec{R}_i}U_{tot}\{\vec{R}_i\} + \vec{\xi}_i, \tag{6}$$

where $\vec{R}_i$ is the position of coarse-grained particle i and ζ represents the friction constant. $\vec{\xi}_i$ is the thermal noise force, which satisfies the fluctuation-dissipation theorem $\langle\vec{\xi}_i\rangle=0$ and $\langle\vec{\xi}_i(t):\vec{\xi}_j(t')\rangle=2T\zeta\delta_{ij}\delta(t-t')\boldsymbol{I}$.

We assume that the interaction between a pair of particles is composed of not only a Lennard-Jones (LJ) interaction, but also a spring interaction

$$U_{tot}\{\vec{R}_i\} = U_{LJ}\{\vec{R}_i\} + U_{sp}\{\vec{R}_i\}. \tag{7}$$

Here we employ the 12-6 type of LJ potential between all pairs of particles:

$$U_{LJ}\{\vec{R}_i\} = 4\epsilon\sum_{j(\neq i)}\left\{\left(\frac{\sigma}{|\vec{R}_i-\vec{R}_j|}\right)^{12}-\left(\frac{\sigma}{|\vec{R}_i-\vec{R}_j|}\right)^{6}\right\}, \tag{8}$$

where ϵ and σ represent the strength and length scale of the interaction, respectively.

A key feature of our model is the introduction of U_{sp} to express the transient gel state formed right after a temperature quench, which is a percolated network of the slower components formed by attractive interactions [4,5,9,22,24]. To represent this transient gel state in a coarse-grained manner, we initially put the particles on a triangular lattice, whose interlattice length is l_0, and introduce the spring (harmonic interaction) between the nearest six particles for each particle as $U_{sp}\{\vec{R}_i\}=\frac{1}{2}\kappa\Sigma'_{j(\neq i)}|\vec{R}_i-\vec{R}_j|^2$ [25]. κ is the spring constant (see Sec. II) and $\Sigma'_{j(\neq i)}$ represents the summation over nearest-neighbor pairs. We can say that the particles represent the cross-linking points of a transient gel. Note that the natural length of the spring is set to 0, which indicates that the transient gel at the initial state has already stored the elastic energy $\kappa l_0^2/2$ per spring. This initially stored elastic energy plays a key role in the selection of patterns, as will be shown later.

Because the network is "transient" and not permanent, a spring should be broken faster when stronger tension acts on it. As described above, the disconnection rate of a spring, $p(l)$, is given by $p(l)=t_0^{-1}e^{-\Delta E(l)/T}$. $\Delta E(l)=E_0-\kappa l^2/2$ [see Eq. (5)] is the activation energy for the disconnection of a spring and is a decreasing function of the length l. The more the spring is stretched, the more easily it is broken. Note that the broken spring is never reconnected again. This irreversible disconnection of the spring does not represent that of the covalent bond of polymers, but represents the breakup of the interaction network composed of polymers or colloids [5,7,22]. When all springs are still connected, the particles only move around their initial positions randomly by thermal noise. However, once a spring is disconnected, the mechanical force balance around it is broken, which induces motion of the network. As a result, the neighboring springs are stretched and more easily disconnected. This represents the stress concentration and the resulting breakup of the transient gel. Here we discuss the role of the connectivity of springs. All the work stored in the spring can be used to lower the barrier to escape from the potential well only when the springs are connected with each other. Once the spring is disconnected, the stored energy is dissipated against solvent drag. Note that the dissipation plays an important role only when a spring is irreversibly disconnected. Thus, we can say that the connectivity is a key factor determining whether the stored energy can be used to lower the barrier or not in our model.

In our model, the interfacial tension originates only from the LJ interaction. It makes droplets circular in the very late stage, where the elastic stress does not play any roles. In the transient gel regime, on the other hand, the viscoelastic stress (spring interaction) overwhelms the interfacial tension (LJ interaction). Thus, the interfacial tension does not play an important role in the pattern selection there. In a polymer solution, however, the final disruption of a string occurs due to the Rayleigh instability. In our model, the switching from the elastic-stress-dominated to the interfacial-tension-dominated regime occurs discontinuously, reflecting the discrete nature of the disconnection of a spring. Thus, our model cannot describe the hydrodynamic breakup process of a string due to the Rayleigh instability. However, this itself

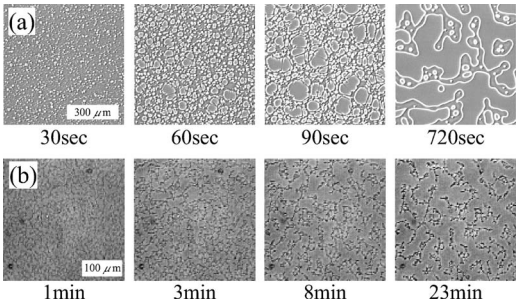

FIG. 2. Phase-separation processes of critical polymer solutions (polystyrene–diethyl malonate) observed by phase-contrast microscopy [26]. Molecular weight M_w, critical concentration ϕ_c, critical temperature T_c, and quenched temperature T_q employed in the experiments are (a) $M_w=8.0\times10^5$, $\phi_c=4.98$ wt %, $T_c=294.0$ K, and $T_q=284.0$ K, (b) $M_w=8.5\times10^6$, $\phi_c=1.2$ wt %, $T_c=301.1$ K, and $T_q=297.0$ K, respectively.

does not affect the pattern evolution so seriously [compare Figs. 2(a) and 3(a)]. Our model can, on the other hand, well describe the breakup process of a network made of colloidal particles or dense polymer droplets. Note that in these systems the string size is comparable to the particle size and thus the coarse-graining hydrodynamic description is not applied; the Rayleigh instability does not play any important role in this case. We emphasize that the characteristics of pattern evolution in viscoelastic phase separation originate from the self-induced elastic stress and its release accompanying the dissipation: Our model mimics the former by a spring and the latter by its disconnection.

Hereafter, we scale the length, energy, and time by l_0, $\kappa l_0^2/2$, and t_0, respectively. The scaled value of a variable X is denoted as $\tilde{X}$. We also scale the frictional constant ζ as $\tilde{\zeta}=\zeta/(\kappa t_0)$. We solve Eq. (6) by using the explicit Euler method. We employed t_0 as the time increment; and thus the disconnection process is performed for every spring per time step (t_0). The disconnection of springs is a thermal activation process. Thus we assume that a spring is disconnected if a randomus generated number, which is uniformly distributed between 0 and 1, is smaller than $e^{-\Delta E(l)/T}$. For all the following simulations, we employ the parameters of the LJ potential as $\tilde{\epsilon}=4$ and $\tilde{\sigma}=0.25$. We solve Eq. (6) for 2500 particles

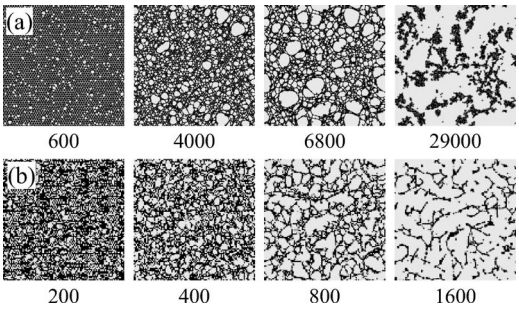

FIG. 3. Temperature ($\tilde{T}$) dependence of pattern evolution processes of a network of disconnectable springs. $\tilde{T}$=(a) 2.1 and (b) 3.0. The other parameters used are $\tilde{E}_0=25$ and $\tilde{\zeta}=100$. Numbers below pictures represent the scaled time $\tilde{t}$.

using periodic boundary conditions in a two-dimensional space $\{0,50\}\times\{0,25\sqrt{3}\}$.

IV. RESULTS AND DISCUSSIONS

A. Basic features of pattern evolution of a network of disconnectable springs

First we show two types of pattern formation processes of a polymer solution experimentally observed with phase-contrast microscopy in Fig. 2. The samples used in the experiments are critical binary mixtures of polystyrene and diethyl malonate. The molecular weights of polystyrene in Figs. 2(a) and 2(b) are $M_w=8.0\times10^5$ and 8.5×10^6, respectively. The darker phase is the polymer-rich phase. Since the phase diagram of a polymer solution is quite asymmetric, the final equilibrium volume fraction of the polymer-rich phase is rather small. Nevertheless, the polymer-rich phase transiently forms a network structure during phase separation. The pattern evolution is characteristic of VPS [4,5,8].

Next we compare our simulation results with the above experimental results. Figures 3(a) and 3(b) show two examples of pattern evolution of VPS, which look similar to the pattern evolution in Figs. 2(a) and 2(b), respectively. Here particles and springs are drawn by black dots and lines, respectively. Note that the springs are more easily disconnected at a higher temperature $\tilde{T}$ [see Fig. 3(b)] than at a lower one [see Fig. 3(a)]. If we regard the black and white regions in Fig. 3 as the more and less viscoelastic phases, respectively, the pattern evolution simulated by our disconnectable spring model reproduces almost all the essential features of VPS. This suggests that our simple model captures the essential features of VPS [4]. Hereafter we study the hole formation and the growth of holes more quantitatively.

Figure 4 shows the temporal change of the average length $\langle\tilde{l}\rangle$ (a) and the length dispersion $\delta\tilde{l}$ (b) of the connected springs for simulations with different $\tilde{E}_0$. For all the cases, $\langle\tilde{l}\rangle$ monotonically decreases with time, which indicates that the stored elastic energy is released by the disconnection of springs. Their final value ($\langle\tilde{l}\rangle\approx0.25$) corresponds to $\tilde{\sigma}$. For smaller $\tilde{E}_0$, $\langle\tilde{l}\rangle$ decreases faster. This means that the springs are more easily broken for smaller $\tilde{E}_0$. Unlike $\langle\tilde{l}\rangle$, $\delta\tilde{l}$ increases in the early stage but then decreases later. Since the dispersion reflects the inhomogeneity of the elastic force, we can say that it is a measure of the strength of the mechanical force created in the network. Thus, the behavior of $\delta\tilde{l}$ in Fig. 4(b) is quite consistent with the fact that the strength of the mechanical force exhibits a peak at a certain time in our previous simulations based on a two-fluid model [12,13].

In the early stage, most of the springs are still connected under thermal noise forces and their lengths are about l_0. The probability that a spring is still connected at a time t is approximated as $(1-e^{-\Delta E(l_0)/T})^{t/t_0}$. Then the characteristic time of the disconnection of a spring can be chosen to be the time t_n at which this probability becomes equal to $1-e^{-1}$. Since $e^{-\Delta E(l_0)/T}\ll1$ in our simulations, this time t_n is approximated as $t_n\approx t_0e^{\alpha-1}$, where $\alpha=\Delta E(l_0)/T$. This t_n can be regarded as

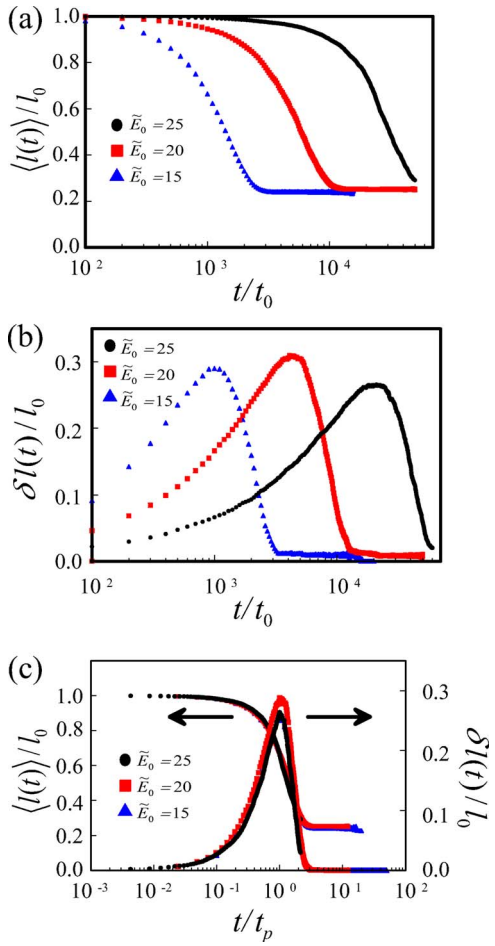

FIG. 4. (Color online) Temporal change in $\langle \tilde{l} \rangle / l_0$ (a) and $\delta \tilde{l} / l_0$ (b) of the connected springs for different $\tilde{E}_0 = 25$, 20, and 15. $\tilde{T} = 1.8$ and $\tilde{\zeta} = 10^2$. (c) Temporal change in $\langle \tilde{l} \rangle$ and $\delta \tilde{l}$ after the scaling.

the characteristic incubation time for hole formation, which can be regarded as nucleation of a droplet. We confirm that the curves of $\langle \tilde{l} \rangle$ and $\delta \tilde{l}$ in Figs. 4(a) and 4(b) can be collapsed on single master curves, if the elapsed time is scaled by t_p, at which $\delta \tilde{l}$ has a peak, as shown in Fig. 4(c). This scaling suggests that $t_p \propto t_n$. Since the mechanical force becomes strongest at t_p, t_p can be regarded as the time when droplets of the less viscoelastic phase strongly interact with each other and thus the network is maximally deformed.

B. Dependence of pattern evolution on α

Figure 5 shows how the domain morphology of VPS at t_p depends upon the parameter α. Since t_n^{-1} controls the hole formation rate of the less viscoelastic phase and $t_n \approx t_0 e^{\alpha - 1}$, we can see from Fig. 5 how the hole formation rate affects the characteristics of the domain pattern. Although the temporal change of $\langle \tilde{l} \rangle$ can be scaled by t_p (or t_n) [see Fig. 4(c)], the characteristics of the pattern do depend upon t_n crucially. Figure 5 clearly indicates that the pattern at t_p is coarser and more inhomogeneous for larger α, whereas it is finer and more homogeneous for smaller α. For a small hole formation

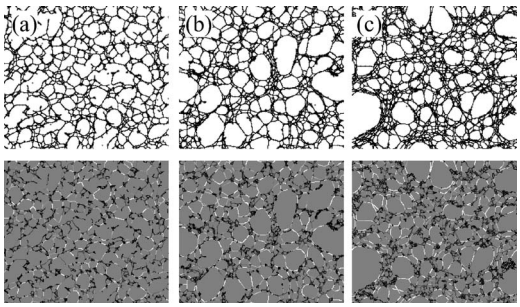

FIG. 5. The α dependence of domain patterns of VPS at t_p; α =(a) 8.3, (b) 10, and (c) 12. The other parameters are $\tilde{T} = 1.8$ and $\tilde{\zeta} = 10^2$. The figures in the bottom row show the spatial distribution of forces acting on each spring. The brighter and darker springs are longer and shorter than l_0, respectively. The brightness of the spring whose length is l_0 is set to be the same as that of the background (i.e., the solvent-rich phase).

rate (large t_n or large α), both position and time, at which each hole is formed, are randomly distributed, which makes the pattern at t_p coarse and inhomogeneous. For small α, on the other hand, the hole formation rate is large and thus most of the holes are formed almost at the same time in the early stage. Thus, the pattern at t_p becomes fine and homogeneous for smaller α.

The images in the bottom row in Fig. 5 show the spatial distribution of the forces acting on springs. Each picture in the bottom row corresponds to that in the top row in the same column. The brightness of springs reflects the spring length; the brighter and darker springs are longer and shorter than l_0, respectively. From Fig. 5, we can see that the fibril-like parts of the network are stretched and the bulk parts of the more viscoelastic phase, which are composed of connected springs, shrink to reduce the stored elastic energy. Therefore, it is expected that fibril-like parts are easily disconnected. We also note that the stress distribution becomes more inhomogeneous for larger α.

C. Dependence of pattern evolution on $\tilde{\zeta}$

Figure 6 shows the $\tilde{\zeta}$ dependence of the characteristic domain pattern and the corresponding stress distribution for the

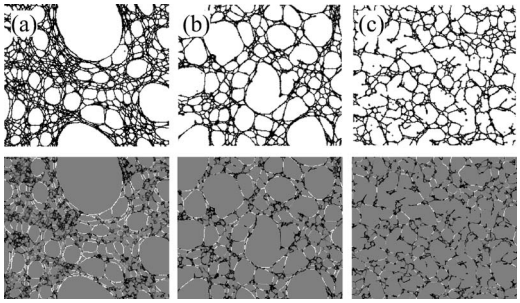

FIG. 6. The $\tilde{\zeta}$ dependence of domain patterns of VPS at t_p for $\alpha = 14$ and $\tilde{T} = 1.8$: $\tilde{\zeta} = 10$, 2×10^2, and 3×10^3 for (a)–(c), respectively. The figures in the bottom row show the spatial distribution of forces acting on each spring.

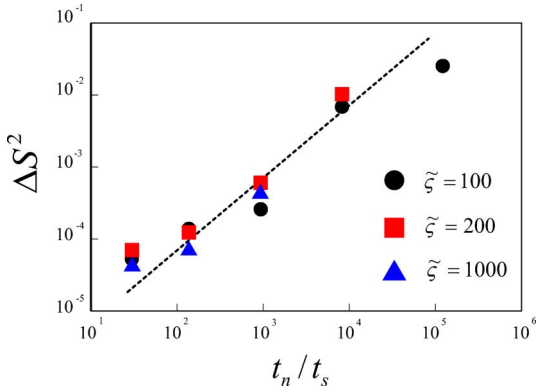

FIG. 7. (Color online) Dependence of the dispersion of the areas of holes (nucleated droplets) ΔS^2 on t_n/t_s for different $\tilde{\zeta}$.

fixed α. The $\tilde{\zeta}$ is a parameter controlling the motion of particles. Our simulations show that the pattern is coarser and more inhomogeneous for smaller $\tilde{\zeta}$, whereas it is finer and more homogeneous for larger $\tilde{\zeta}$. In our model, the characteristic time of the particle motion connected by a spring is given by $t_s=\zeta/\kappa$. Thus, t_s^{-1} controls the growth speed of a hole (i.e., the solvent-rich droplet). A simple physical consideration leads us to a conclusion that one of the most important factors controlling the domain morphology of VPS is the ratio of the growth rate to the creation rate of droplets, t_n/t_s. This conclusion is supported by Fig. 7, which shows the t_n/t_s dependence of the dispersion of the areas of holes ΔS^2. ΔS^2 is calculated as $\Delta S^2=\langle S^2\rangle_a-\langle S\rangle_a^2$. Here $\langle X\rangle_a=\Sigma_i X_i S_i/\Sigma_i S_i$ means the averaged value of X weighted by each area S_i, which represents the area of the hole labeled i. We find the relation $\Delta S^2 \propto t_n/t_s$. Although the physical meanings of this power law and the exponent are not clear now, this result indicates that t_n/t_s is a key parameter controlling the morphology of VPS. The stress distribution of springs is almost the same as those of Fig. 5. In Fig. 6(a), we can see the inhomogeneous stress distribution, which further suggests the existence of spatial correlation in the stress field, which will be discussed later.

D. Dependence of pattern evolution in β

Next we discuss another physical factor controlling the morphology. Using the hole formation rate t_n^{-1}, the disconnection rate can be approximated as $p(l)\approx(t_n/e)^{-1}e^{\beta(\tilde{l}^2-1)}$, where $\beta=\frac{1}{2}\kappa l_0^2/T$ $(=1/\tilde{T})$ is the scaled initially stored elastic energy. Figure 8 shows the dependence of $\Delta E/T$ on l schematically. It indicates that the initially stored elastic energy determines the decreasing rate of the activation energy for an increase in the initial length of springs; note that the slope of $\Delta E(l)/T$ at l_0 is given by -2β (see Fig. 8). The disconnection probability of a spring whose length is $\tilde{l}=(1+1/\beta)^{1/2}$ is enhanced by a factor e. Thus, $1/\beta$ is a measure of how much a spring can be elongated without disconnection. For a system made of springs of smaller β, a spring stores less elastic energy in the initial state, and thus can be more stretched and store more elastic energy before disconnection. On the other hand, for a system made of springs of larger β. a spring cannot be elongated so much and is easily broken. Thus we can say the parameter β represents the fragility of the springs.

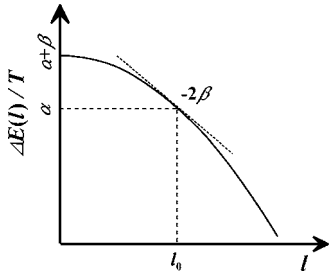

FIG. 8. The l dependence of $\Delta E/T$ $(=\alpha-\beta[(l/l_0)^2-1])$.

Figure 9 shows the β dependence of domain morphology of VPS with fixed t_n/t_s. We can see that the morphology of the droplets is rather circular for small β, while it is rather anisotropic for large β. For a fixed value of t_n, which is the case of Fig. 9, $\beta^{-1/2}$ can also be regarded as the width of the distribution of $p(l)$. For small β, the disconnection probability $p(l)$ depends on $\tilde{l}$ gradually, and thus springs of various lengths can coexist. In other words, the disconnection process is probabilistic. For large β, on the other hand, the dependence of $p(l)$ on length l is rather sharp and thus the disconnection process is deterministic. In this sense, the simulations of large and small β correspond to a fragile solid and a viscoelastic fluid, respectively.

Figure 10 shows the β dependence of the shape of a droplet of the less viscoelastic phase and its stress distribution. Initially we disconnect ten springs on a horizontal straight line, which behaves as a nucleus of the less viscoelastic phase. Since we used a larger value of α (=30) in these simulations, the disconnection rate of springs is very small in the matrix and thus we do not see any spontaneous disconnection events in the matrix during the simulation time. For larger β, the anisotropic growth of the nucleus is quite similar to that of fracture in an elastic solid [see Fig. 10(a)]. On the other hand, it has a circular shape for smaller β [see Fig. 10(d)]. From the pictures in the bottom row, we can see that the stress is more concentrated and localized for larger β, whereas it is more homogenized and delocalized for smaller β.

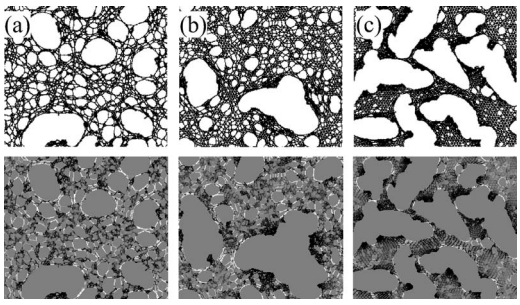

FIG. 9. The β dependence of domain patterns of VPS at t_p for $\alpha=12$ and $\tilde{\zeta}=10^2$; $\beta=0.91$, 1.5, and 3.6 for (a)–(c), respectively. The figures in the bottom row show the spatial distribution of forces acting on each spring.

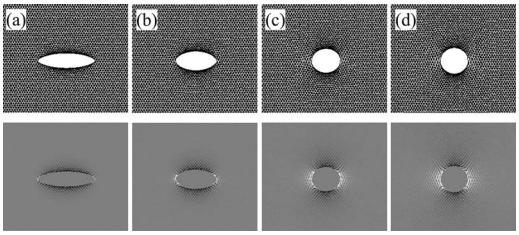

FIG. 10. Shape of a single growing hole (droplet) (top row) and the force distribution around it (bottom row) for $\alpha=30$ and $\tilde{\zeta}=10^2$; $\beta=5,2,1,0.5$ for (a)–(d). All the holes (droplets) have almost the same area. As initial conditions, we disconnect ten springs along a horizontal line. These initially broken springs can be regarded as an anisotropic nucleus of crack.

Disconnection of a spring leads to the loss of the force balance condition around it. Therefore, the neighboring springs are more stretched and eventually disconnected. For large β, springs that are stretched larger than l_0 are necessarily disconnected, while springs shorter than l_0 remain connected. For this rather deterministic process, the disconnection process is similar to a crack propagation in the fracture of solids. The springs at the edge of an anisotropic droplet, where the mechanical stress is concentrated, are selectively disconnected so as to release the elastic energy efficiently. This makes the shape of a hole (or a droplet) more anisotropic. Such patterns are indeed observed experimentally in VPS, as will be reported elsewhere. For small β, on the other hand, the stretched springs are not disconnected easily and cannot release the elastic energy at the front of a crack. Thus, the droplet becomes rather isotropic and circular to satisfy the force balance among the springs on the periphery.

E. Spatial correlation in hole formation

Next we discuss other interesting characteristics of pattern formation in VPS. One-dimensional arrays of droplets are often formed in the simulations [see Fig. 11(a)]. A similar pattern is also often observed in experiments (see Fig. 2). This indicates the presence of elastic coupling among holes (i.e., droplets). Figure 11(b) schematically shows such an array of nucleated solvent-rich droplets and the forces acting on the shrinking transient gel. The formation of a droplet array can be explained as follows. If two droplets are nucleated close to each other at about the same time, the deformation field around them [see Fig. 11(b)], which is induced by the shrinking of the more viscoelastic matrix phase, becomes anisotropic. The stress is more concentrated at the edges of the array of droplets. This helps creation of holes there [see the hatched regions in Fig. 11(a)], and thus leads to a further increase in the number of droplets in the array. The overall domain shape of the array is approximated by an elongated ellipsoidal droplet [see the ellipsoid of the broken line in Fig. 11(a)], if we neglect the thin bridges between droplets. Note that the growth process of this ellipsoidal droplet resembles the fracturelike growth of a nucleated droplet observed in simulations of large β [see Fig. 9(c)].

F. How do the characteristics of the interaction potential affect pattern evolution?

Finally, we discuss the relationship between the interaction potential between the slower components of a mixture and the resulting domain pattern of VPS. As shown in Sec. II, α and β are approximated as $\alpha=\epsilon_p^*-\frac{1}{2}-\ln\frac{N_p-\beta}{}$ and $\beta=(6\epsilon_p^*/\delta^2)(l_0/N_pb)^2$, where $\epsilon_p^*=\epsilon_p/T$ and $\delta=\sqrt{2\epsilon_p/\kappa_p}/b$ are the scaled strength and width of the interaction potential between the particles composing springs, respectively. The α is an increasing function of ϵ_p^*. As shown above, α represents the amount of elastic energy that each spring can further store before disconnection. This suggests that the domain pattern becomes coarser and more inhomogeneous when the interaction between particles (or molecules) of the slower component in a mixture is strong. Since α decreases with increasing N_p, the domain pattern should be more inhomogeneous when the density of cross-linking points in the initial transient gel state is higher. β is the scaled elastic energy stored by the initial spring and controls the fragility of the spring. Therefore, the larger the elastic energy stored in the initial network structure (i.e., the larger l_0/N_pb), the larger the fragility becomes. The β is a decreasing function of the width of the potential well, δ. Therefore, if the interparticle potential is steeper, the fragility of springs should be larger and the resulting domain pattern should become more anisotropic. This suggests that we may intentionally control the domain pattern of VPS by changing the interaction potential between the components.

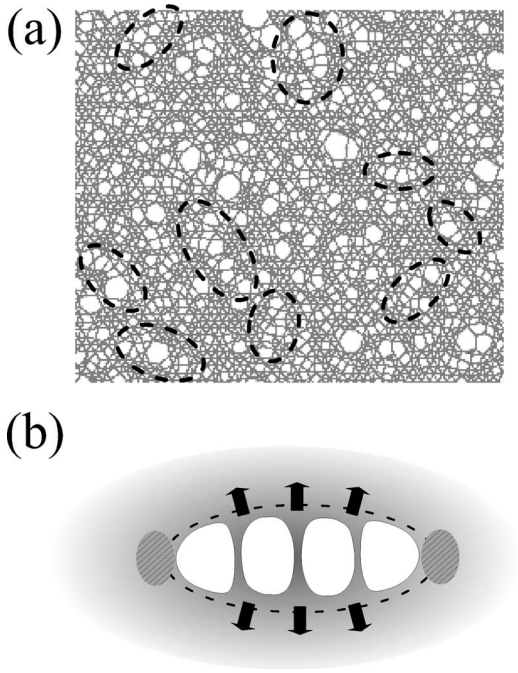

FIG. 11. (a) Arrays of nucleated droplets observed in the simulation of $t_n/t_s=920$, $\beta=0.56$, and $\tilde{t}=5\times10^3$. (b) Schematic picture of an array of nucleated droplets and the stress field in the shrinking viscoelastic matrix phase.

V. SUMMARY

In summary, we demonstrate that the essential features of the pattern evolution of a transient gel (namely, VPS) can be captured by a very simple toy model, in which Brownian particles are connected by disconnectable springs. Our simu-

lations very well reproduce the characteristics of pattern evolution of VPS observed experimentally. This suggests that the basic mechanism of the coarsening of the pattern in VPS is the stress concentration and the resulting breakup of the stretched network under thermal fluctuations. Our simulations indicate that there are two key parameters controlling the network morphology of VPS: the ratio of the growth rate to the nucleation rate of a droplet of the less viscoelastic phase (t_n/t_s) and the fragility of the network (β).

We also show how the characteristics of the interaction potential of particles composing a network control the two key parameters α and β. When the interaction between particles is stronger, the resulting domain pattern becomes coarser and more inhomogeneous. The density of the cross-linking points in a transient network also affects the domain morphology. The width of the potential and the conformation entropy of the chain affect the fragility, which controls the anisotropy of droplets. This information may be of technological importance for the morphology control of a network structure produced by VPS.

Finally, we mention that the phenomena simulated here may have a close connection to those of fracture of viscoelastic matter [27,28].

ACKNOWLEDGMENTS

The authors are grateful to Dr. Takehito Koyama for providing the experimentally observed pattern of VPS. This work was partly supported by a Grant-in-Aid for Scientific Research from the Ministry of Education, Culture, Sports, Science and Technology, Japan.

[1] H. Tanaka, Macromolecules **25**, 6377 (1992).
[2] H. Tanaka, Phys. Rev. Lett. **71**, 3158 (1993).
[3] H. Tanaka, J. Chem. Phys. **72**, 4756 (1994).
[4] H. Tanaka, J. Phys.: Condens. Matter **12**, R207 (2000).
[5] H. Tanaka and T. Araki, Chem. Eng. Sci. (to be published).
[6] A. Onuki, *Phase Transition Dynamics* (Cambridge University Press, Cambridge, U.K., 2002).
[7] H. Tanaka, Y. Nishikawa, and T. Koyama, J. Phys.: Condens. Matter **17**, L143 (2005).
[8] H. Tanaka, Phys. Rev. Lett. **76**, 787 (1996).
[9] H. Tanaka, Phys. Rev. E **59**, 6842 (1999).
[10] H. Tanaka and Y. Nishikawa, Phys. Rev. Lett. **95**, 078103 (2005).
[11] T. Taniguchi and A. Onuki, Phys. Rev. Lett. **77**, 4910 (1996).
[12] H. Tanaka and T. Araki, Phys. Rev. Lett. **78**, 4966 (1997).
[13] T. Araki and H. Tanaka, Macromolecules **34**, 1953 (2001).
[14] T. Okuzono, Phys. Rev. E **56**, 4416 (1997).
[15] C. Sagui, L. Piche, A. Sahnoune, and M. Grant, Phys. Rev. E **58**, 4654 (1998).
[16] J. Zhang, Z. Zhang, H. Zhang, and Y. Yang, Phys. Rev. E **64**, 051510 (2001).
[17] K. Luo, W. Gronski, and C. Friedrich, Eur. Phys. J. E **15**, 177 (2004).
[18] D. Sappelt and J. Jäckle, Europhys. Lett. **37**, 13 (1997); Physica A **240**, 453 (1997); Polymer **39**, 5253 (1998).
[19] R. Ahluwalia, Phys. Rev. E **59**, 263 (1999).
[20] A. Bhattacharya, S. D. Mahanti, and A. Chakrabarti, Phys. Rev. Lett. **80**, 333 (1998).
[21] H. Liu, A. Bhattacharya, and A. Chakrabarti, J. Chem. Phys. **111**, 11183 (1999).
[22] H. Tanaka and T. Araki, Phys. Rev. Lett. **85**, 1338 (2000).
[23] M. Doi and S. F. Edwards, *The Theory of Polymer Dynamics* (Clarendon Press, Oxford, 1986).
[24] C. B. Muratov, Phys. Rev. Lett. **81**, 3699 (1998).
[25] K. Sekimoto, N. Suematsu, and K. Kawasaki, Phys. Rev. A **39**, R4912 (1989).
[26] T. Koyama, Ph.D. thesis, The University of Tokyo, 2001 (unpublished); and (private communication).
[27] G. Carbone and B. N. J. Persson, Eur. Phys. J. E **17**, 261 (2005).
[28] A. R. C. Baljon and M. O. Robbins, Macromolecules **34**, 4200 (2001).